Submitted To:	U.S. Department of Energy Energy Efficiency & Renewable Energy Vehicle Technologies Office
FOA Name & Number:	Fiscal Year 2017 Vehicle Technologies Program Wide Funding Opportunity Announcement DE-FOA-0001384
Nature of Report:	Final Scientific/Technical Report
Award Number:	DE-EE0007797
Award Type:	Cooperative Agreement
Prime Recipient:	University of Pittsburgh
Prime Recipient Type:	University
Project Title:	Engineering Approaches to Dendrite free Lithium Anodes
Principal Investigator:	Prashant N. Kumta
Team Member:	Moni K. Datta
Team Member:	Oleg. Velikokhatnyi

I. Executive Summary

Lithium (Li) cycling under normal conditions in a lithium metal battery (LMB) witnesses a non-planar Li/electrolyte interface (cellular/dendritic microstructure) primarily responsible for controlling the performance, safety and reliability of LMBs. Dendrite formation in electrochemical systems occurs due to inhomogeneous current densities coupled with local diffusion gradients, surface roughness, and kinetic roughening of the surface of the anode systems. However, as complex and ubiquitous as it seems, the phenomenon of Li dendrite nucleation and growth are not very well-understood. It is reported that a planar front is stable only if the current density is sufficiently small, and/or the transference number as well as/or chemical diffusivity of Li ion in the electrolyte is sufficiently large. Since the surface microstructures form a major link connecting the performance and electrodeposition/plating conditions, it is important to develop scientific understandings of how the Li metal plating conditions, as well as the electrolyte and the current collector properties influence the resulting microstructures of the plated Li metal. This is important in order to predict, modify, and control the microstructure of the deposited Li metal by meticulously designing the appropriate battery components as well as the Li metal electrodeposition/plating conditions. Adding to the complexity and increasing the enigmatic nature is the formation of the solid-electrolyte interphase (SEI). Control and elimination of Li metal dendrite formation is a veritable challenge and, if overcome, would render the universal adoption of lithium metal batteries (LMB) for stationary and transportation electric vehicle (EV) applications. The current project is thus, a scientific study of novel approaches undertaken and implemented to address the highly complex but ubiquitous problem of dendrite formation in LMBs, combined with electrolyte decomposition, and associated cell-failure. Development of dendrite free high-performance Li anodes will enable the use of Li-free cathodes (e.g. Li-S, Li-air) opening up a myriad possibilities pushing the envelope in terms of achieving the desired cathode capacity and battery energy density with cost $\leq$\$75 $(kWh)^{-1}$.

This project will yield lithium metal anodes with specific capacity ~2000 mAh/g (~4 mAh/cm2), cycling stability of ~1000 cycles, coulombic efficiency loss $\leq$ 0.01%, coulombic efficiency: ~99.99% combined with superior rate capability. The goal is to systematically characterize the different approaches identified for the generation of dendrite-free Li-metal anodes while also providing an understanding of the scientific underpinnings, as well as evaluating the microstructure and electrochemical performance of the dendrite free Li metal anodes. The morphological stability/instability criterion analysis will be developed based on the concept of "the constitutional under-potential plating" (CUP) and perturbation analysis occurring at the Li-metal/electrolyte interface to understand the driving force as well as the resistance to perturbation for the formation of the nonplanar interface microstructure. Finally, the effects of battery cycling parameters such as current density and potential gradient on the morphology and size of Li microstructures (e.g. dendrite tip radius, dendrite arm spacing) were developed which effectively predict, modify, and control the microstructure of the deposited Li metal by designing appropriate battery component systems and electrodeposition conditions. Generation of high performance dendrite free Li metal anodes utilizing the approaches developed herein will successfully demonstrate generation of novel sulfur cathodes affording the fabrication of Li-S batteries meeting the targeted gravimetric energy densities [3] 350 Wh/kg and $\geq$750Wh/l with a cost target \$125/kWh and cycle life of at least 1000 cycles for meeting the next generation EV everywhere blueprint.

II. Comparison of Actual Accomplishments with the Project Goals

Table-1: Milestone and Results obtained in budget period 1.

Milestone	Type	Results
Identification of Porous foam materials (PFM) and Multilayer Porous Foam (MPF) materials	Technical	Identified and synthesized porous foams materials and multi-layer porous foam materials with high electronic conductivity, porosity>60%, stability in electrolyte and high pore volume to nucleate lithium in-pore
Synthesize PFMs and MPFs with superior Li^+ conductivity and explore ideal morphologies to ensure complete dendrite prevention and induce cycling stability	Technical	Synthesis of PFMs and MPFs exhibiting; Specific capacity ≥1000 mAh/g (≥4 mAh/cm^2), >400 cycles without cell failure), initial CE: ≥95% with ≤0.05% loss per cycle (LPC).
Perform first principles investigations into identifying electronically and ionically conductive materials capable of acting as structurally isomorphous alloy (SIA) compositions over a range of lithium compositions	Technical	Identified suitable materials for SIA development.
Fabrication and characterization of suitable PFM and MPF electrodes	Go/No Go	Suitable electrodes were designed, fabricated and tested in a coin cell configuration. Specific capacity ≥1000 mAh/g (≥4 mAh/cm^2), ~100 cycles without cell failure)

Table-2: Milestone and Results of budget period 2.

Milestone	Type	Results
Synthesis and testing of SIA electrodes	Technical	Developed SIA materials and electrodes: Specific capacity ≥1400 mAh/g (≥4 mAh/cm^2), >200 cycles, CE, loss per cycle (LPC) ≤0.05%, CE: ≥97%
Design and engineering of high capacity multi-alloy systems, multicomponent alloys (MCAs) and interface engineered copper (IEC) electrodes	Technical	Developed MCAs and IE Cu current collector exhibiting; Specific capacity ≥1000 mAh/g (≥4 mAh/cm^2), ~300 cycles, LPC ≤0.01%, CE: ≥99%.
Optimize PFM/MCA/IEC electrodes to improve capacity and stability for scaling	Technical	Optimized PFM/MCAs/IECs electrodes with improved capacity and stability
Fabrication and characterization of suitable SIA and CMA electrodes	Go/No Go	Half-cell tested SIA/MCA/IEC tested as per AOI6 requirements with Specific capacity≥1400 mAh/g (≥4 mAh/cm^2), >200 cycles, CE, LPC ≤0.05%, CE: ≥97%

Table-3: Milestone and Results of budget period 3.

Milestone	Type	Description
Integrated electrode (IE) generation by tying together the three different trees of development 'i.e. coating development/PFM, MPF development/SIA exploration by optimizing to maximize lithium content with no dendrite formation over extended cycling, especially at high rates to demonstrate high capacity	Technical	Generation of final deliverable high energy density IE: High capacity ≥2000 mAh/g (≥4 mAh/cm^2), ~400 cycles, CE, LPC ≤0.01%, CE: ≥99.99% with superior rate capability.
Fabrication of the desired 10 mAh full cell	Technical	75-100 μm thick electrodes of Li-S battery designed, fabricated and tested in coin cell, pouch cell and full-cell configurations and compared to desire AOI6 volumetric energy density requirements
Fabrication of the desired 10 mAh full cell	Technical	AOI6 deliverable

Phase – 1 (budget period 1) of the current project was aimed at the development of porous foam materials (PFMs) and multilayer porous foam materials (MPF) with the aim of reducing orthogonal lithium nucleation and growth. Porous metal foams were prepared by electrochemical etching method with varying amounts of hierarchical porosity/wall roughness (**Figure 1a**). **Figure 1b** shows attempts at the use of this innovative architecture to inhibit the formation of Li-dendrite during cycling (i.e., porous metal foams (PMFs) as novel dendrite resistant electrodes).

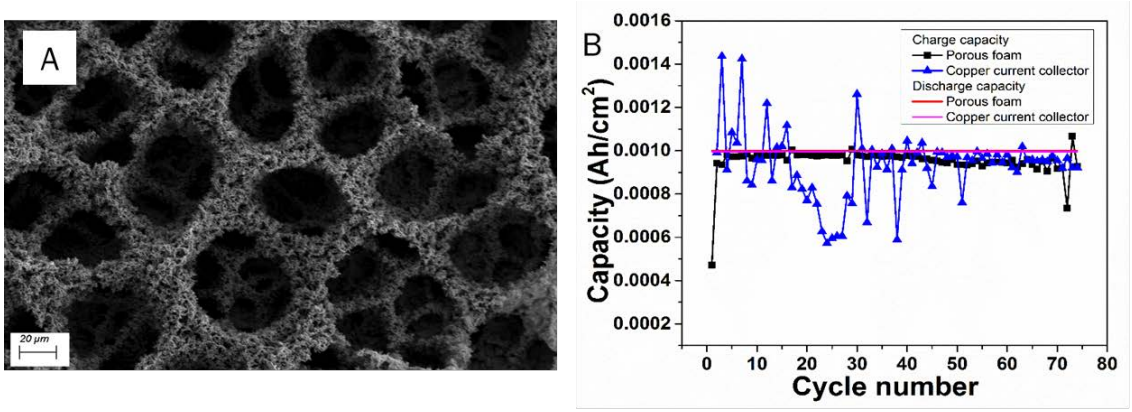

Figure 1: (a) Electrochemically prepared porous metal foam (PMF). (b) Improvement in coulombic efficiency afforded by the use of porous metal foam architectures.

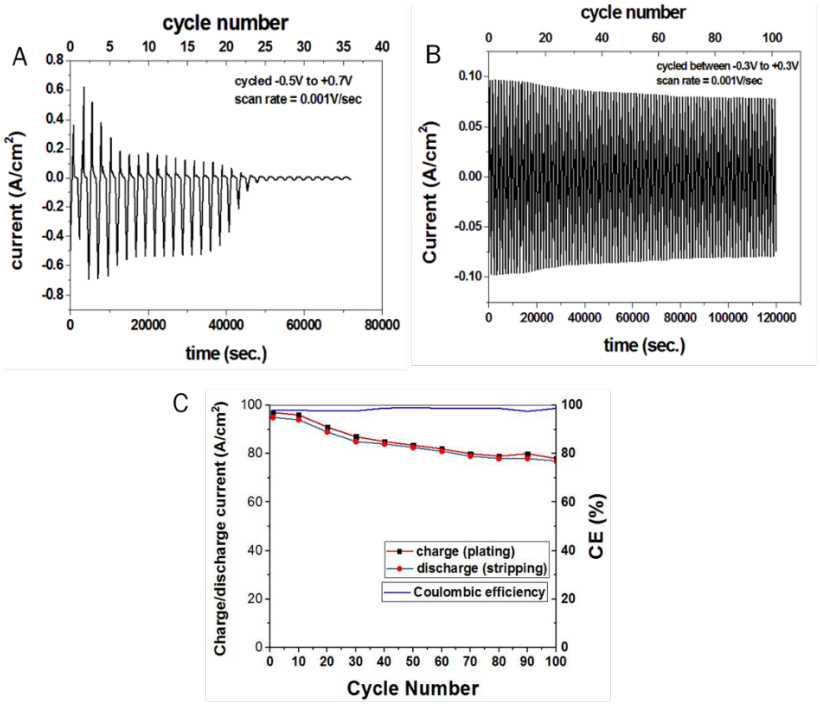

Figure 2: Current-time profiles of cyclic voltammetry of (a) lithium-copper current collector cell (b) lithium-Li-SIA cell; (c) Coulombic efficiency of Li-SIA cell showing stability thereof.

Figure 2 shows the effect of using structurally isomorphous alloys (SIA) as electrodes for lithium metal plating/de-plating in comparison to traditional copper current collector. It can be seen in **Figure 2a** that upon cycling lithium metal on a copper current collector (cyclic voltammetry), most of the lithium is consumed via dendrite formation and solid electrolyte interphase (SEI) occurrence. On the other hand, it can be seen in **Figure 2b** and **Figure 2c** that the SIA electrodes exhibit excellent charge retention as well as coulombic efficiency over extended cycling at very high current densities on the order of ~80-100 mA/cm^2.

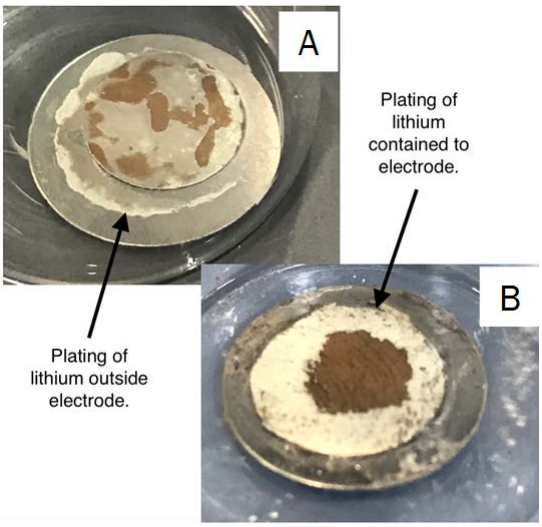

Figure 3: (a) Formation of lithium on stainless steel spacer in coin cell tests (b) Diffusion pathways causing plating of lithium on polymeric coated stainless-steel spacers.

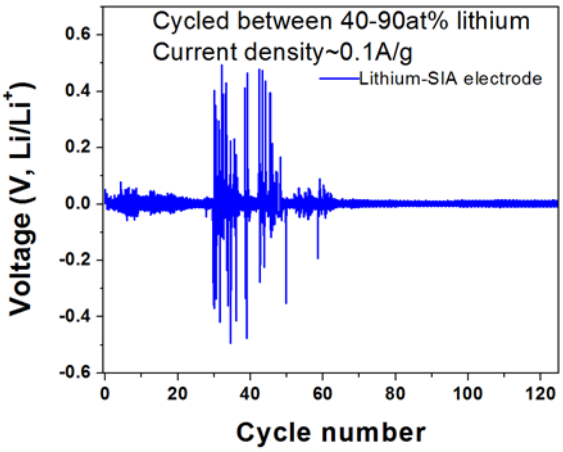

Figure 4: SIA electrodes demonstrate long-term stability though there is a rise in overpotential due to possible phase segregation.

It was, however, observed during post-cycling that the lithium dendrites tend to deposit at the edge of the porous foam materials since the separator contacts the stainless-steel spacer behind the foam structure (**Figure 3a**). This issue was partially resolved by applying non-conductive polymeric coating barriers to the spacer (**Figure 3b**). **Figure 4** demonstrates long-term cycling of

34 mAh/cm^2 at 1.6 mA/cm^2 using the SIA electrodes. Overpotential of ±30-100 mV is maintained for ~30 cycles with visible instabilities observed in the 30-60 cycles after which the overpotential is stabilized in the range of ± 12-15 mV for over 120 cycles. The intermediate instability region is possibly due to phase segregation and compositional inhomogeneity as observed in **Figure 4**.

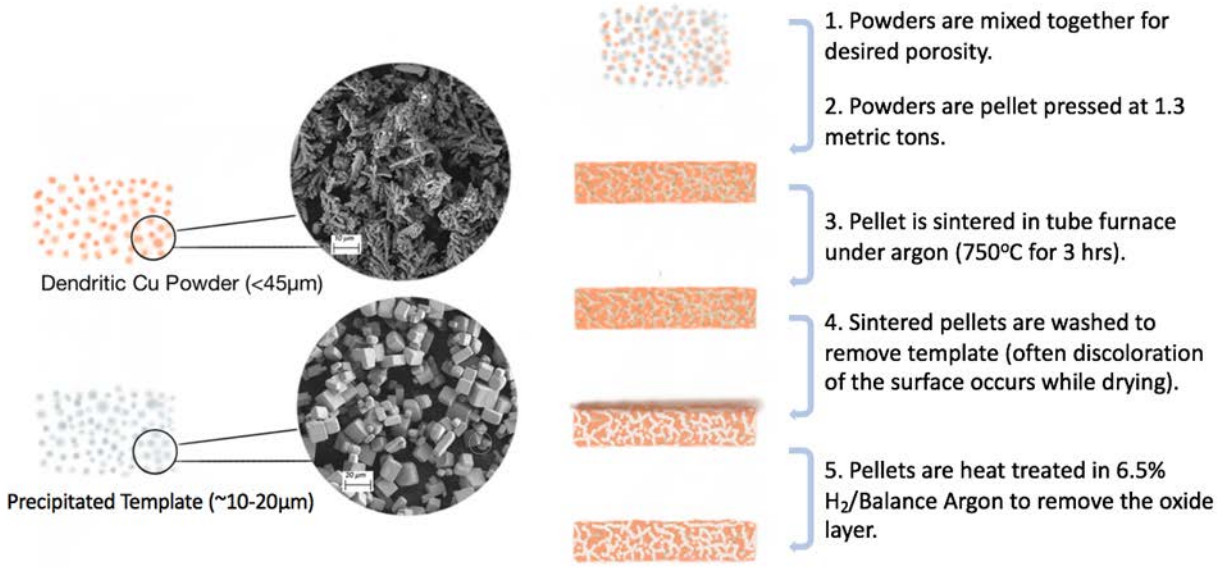

Figure 5: Preparation method for Gen-2 porous metal foams.

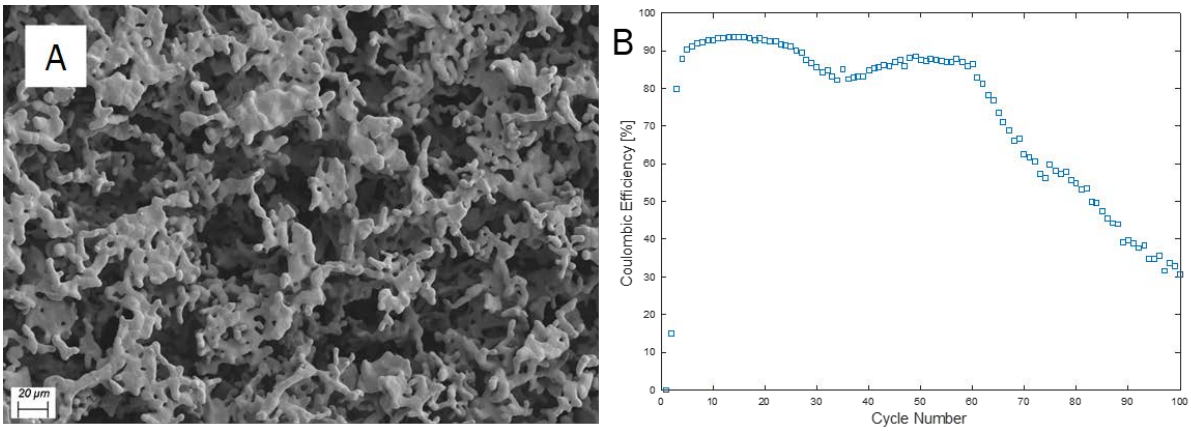

Figure 6: (a) SEM image of the high porosity (~85%) Cu foams after sintering and removal of the sacrificial template. (b) Gen-2 Cu Foam electrodes demonstrate stable cycling region of 60 cycles at ~90% coulombic efficiency.

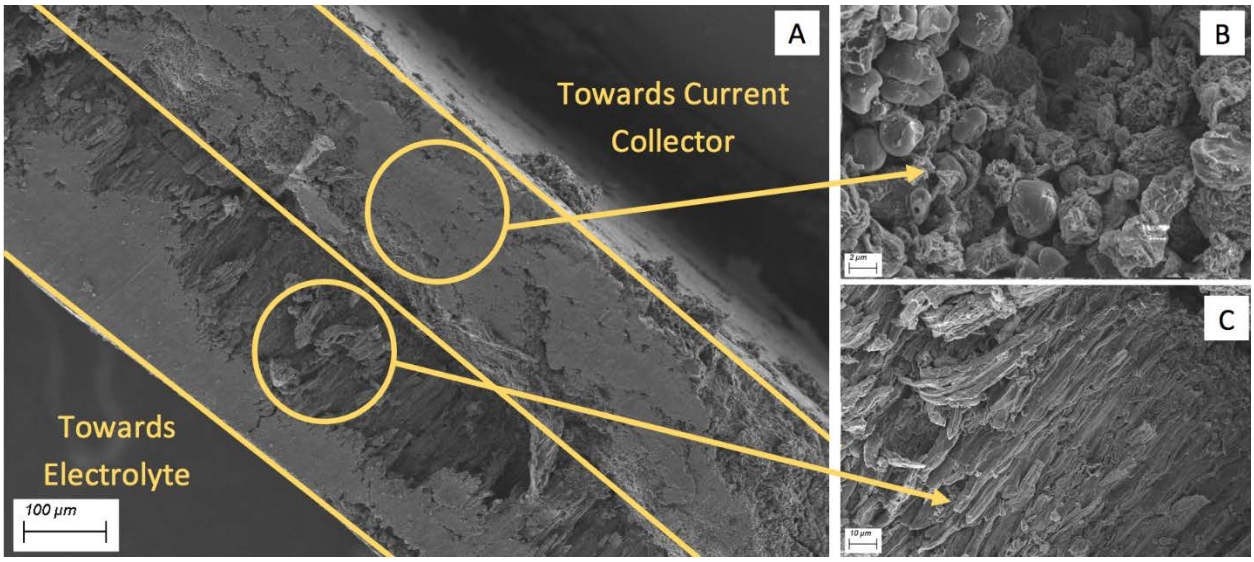

Figure 7: SEM images of the porous Cu foam electrodes after cycling (~200 cycles). (A) Cross-section view, (B) Close up of lithium deposited within the foam structure, and (C) Close up of lithium deposited on top of the foam surface following pore closure by competitive SEI formation in the foam structure.

Following Q1-2017 and Q2-2017, research migrated to Gen-2 PMFs with easily controlled porosities of up to 90% generated using the sacrificial template approach outlined in **Figure 5**. **Figure 6a** shows the SEM image of the Gen-2 PMFs after sintering and removal of the sacrificial template. A continuous network of pores (porosity ~85%) is observed. **Figure 6b** shows the cycling efficiency of Li plating and deplating on Gen-2 Cu foams at a current density of 1 mA/cm^2 for 1 h with a deplating cutoff voltage of 1V in 1.8 M LiTFSI, 0.1 M $LiNO_3$ in DOL:DME (50:50 vol.) electrolyte. The Cu foams demonstrate stable cycling to 60 cycles with a columbic efficiency of ~90% after which they transition into a region of constant fade similar to Li plating/deplating seen on the Cu foil. This transition from stable cycling to constant fade is attributed to transition of the globular Li plating morphology within the porous architecture to a columnar morphology forming on the foam surface. **Figure 7a** shows the cross section of the cycled foam electrodes. **Figure 7b** and **Figure 7c** show the different deposition morphologies in each region attributed to competitive SEI layer formation.

The work of this project thus far was involved in attempts at controlling the formation of the SEI layer and limiting growth during extended cycling. Unfortunately, increasing the thickness of the PMFs offered only minimal increase in the number of achievable stable cycles, with almost no difference being shown when increasing from 80mg of active material to 120mg of active material. The SEI formation periodically would result in closure of the pores thus resulting in eventual dendrite formation rather than annihilation of the dendrites therefore resulting in eventual failure. Work was therefore performed on surface modification of the porous metal foams through the use of additives to address this same problem. Initial unoptimized studies have yielded

promising results, increasing the coulombic efficiency from 95% to 99% and the number of stable cycles from ~60 cycles to ~100 cycles.

Metal Porous Foams:

In the budget period 1 porous Cu foams have shown improved stability over plain Cu foils in terms of achieving stable plating efficiencies. However, the foams suffer from unstable Li plating and buildup of solid electrolyte interphase (SEI) layers that eventually result in instabilities causing cycling fade and loss in capacity. Efforts for phase-2 (budget period 2) of the project have focused on modifications to the surface of the metal porous foams (MPFs) in order to control SEI formation and growth, specifically the use of a thin organic and lithium-ion conducting coatings.

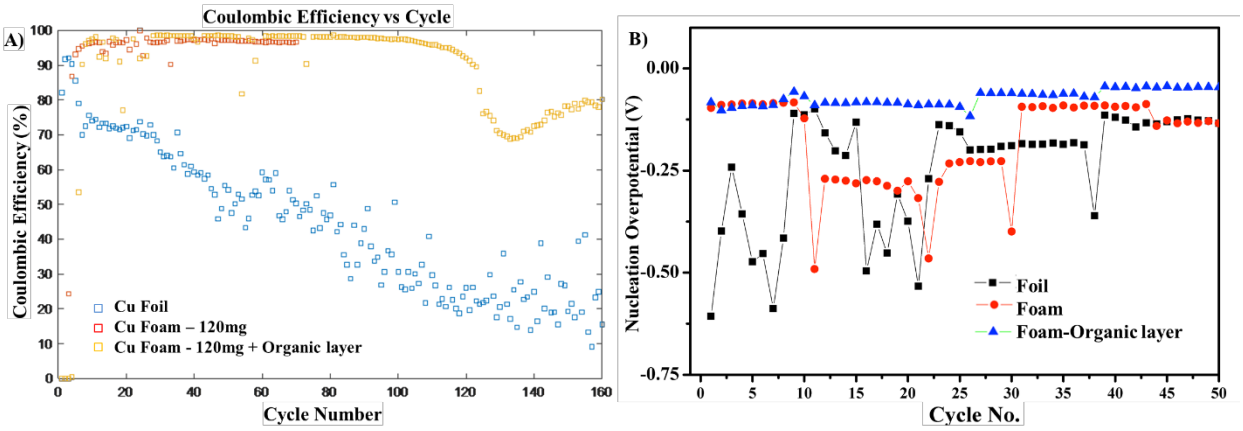

Figure 8: a) Coulombic Efficiency of Li plating on MPF with organic coating, without coating, and on an unmodified copper foil. b) Nucleation overpotential for Cu foil, Cu foam, and

As shown in **Figure 8a**, the use of organic layers embedded MPF improves the coulombic efficiency of the electrode and increases the number of stable cycles achieved before fade (~70 cycles for unmodified MPF to ~120 cycles for the organic layer containing MPF). Furthermore, a drop in the nucleation overpotential of lithium was observed with the addition of this organic layer (**Figure 8b**).

The erratic behavior of the nucleation overpotential observed for the unmodified foam and the copper foil can be attributed to the instabilities of the SEI layers formed continuously on the metallic copper surface. The addition of the organic layer results in the formation of a more stable SEI layer combined with providing solid state Li^+ diffusion pathways, thus, together reducing the overall deleterious influences of the SEI and resulting in improved reversible lithium plating with lower resistance to ionic conduction. Eventually, however, the SEI layer grows too thick and a coulombic efficiency fade is eventually observed leading to capacity loss. Additional work was therefore done to improve the uniformity of the organic coating, as well as examine the addition of other surface additives to assist in the formation of a stable SEI or act as an artificial SEI. The wetting of the Li metal on Cu also influences the stability and plating morphology of Li plating and hence, work was focused to develop zero nucleation potential next generation anode substrate materials to replace Cu as novel dendrite-free substrates as described in another section (Zero Nucleation Potential Electrodes) in the sections to follow.

Surface Modification of Li Metal:

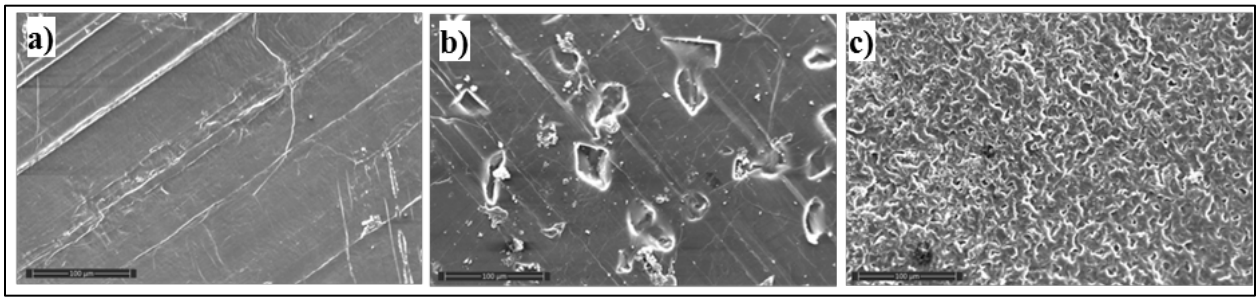

Figure 9: SEM images of (a) pristine lithium foil, (b) lithium foil imprinted with 300 grit sandpaper, and (c) 2500 grit.

The surface of pristine lithium (P-Li) foil is modified by using various media corresponding to different grits (300 grit to 2500 grit) on the surface and the effect of surface modification on the nucleation and growth of lithium on the lithium foil was studied. **Figure 9** shows the SEM of the surface pattern generated with different degrees of roughness developed by using the surface patterning technique. By modifying the surface roughness, high energy sites for preferential plating can be obtained, thus controlling the plating location and morphology preventing both dendrite and high surface area lithium.

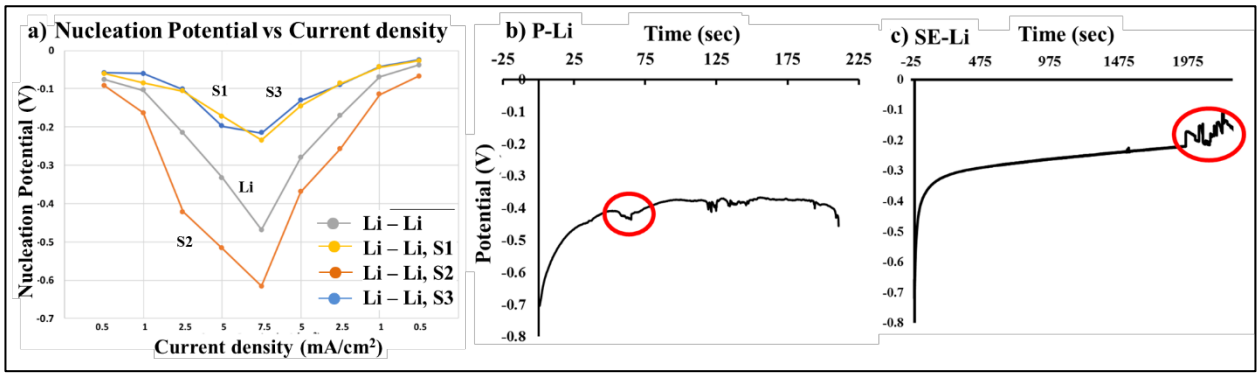

Figure 10: a) Nucleation potential for various surface modified lithium-metal foils at different current densities. Sand's time experiment showing potential vs time for symmetric Li/Li cells for a)P-Li and b) SE-Li.

A reduction in nucleation overpotential is observed for the 300-grit imprinted lithium, however, the overpotential is unaffected when using the 2500-grit sand paper. The deep sites obtained by the 300-grit sandpaper provide a pre-active high energy sites for nucleation thus reducing the overpotential during Li plating. (**Figure 10**) shows the nucleation potential as a function of current density for many of the modified lithium surfaces (S1, S2, and S3). It is observed that large modifications in the engineered surface area (S1 and S3) of the grooved structures created on the surface of the lithium metal helps to lower the nucleation potential. On the other hand, creation of small modification of the surface architecture and morphological structures create an undesired roughness and surface characteristics that actually increase the nucleation potential compared to the unmodified lithium-metal surface.

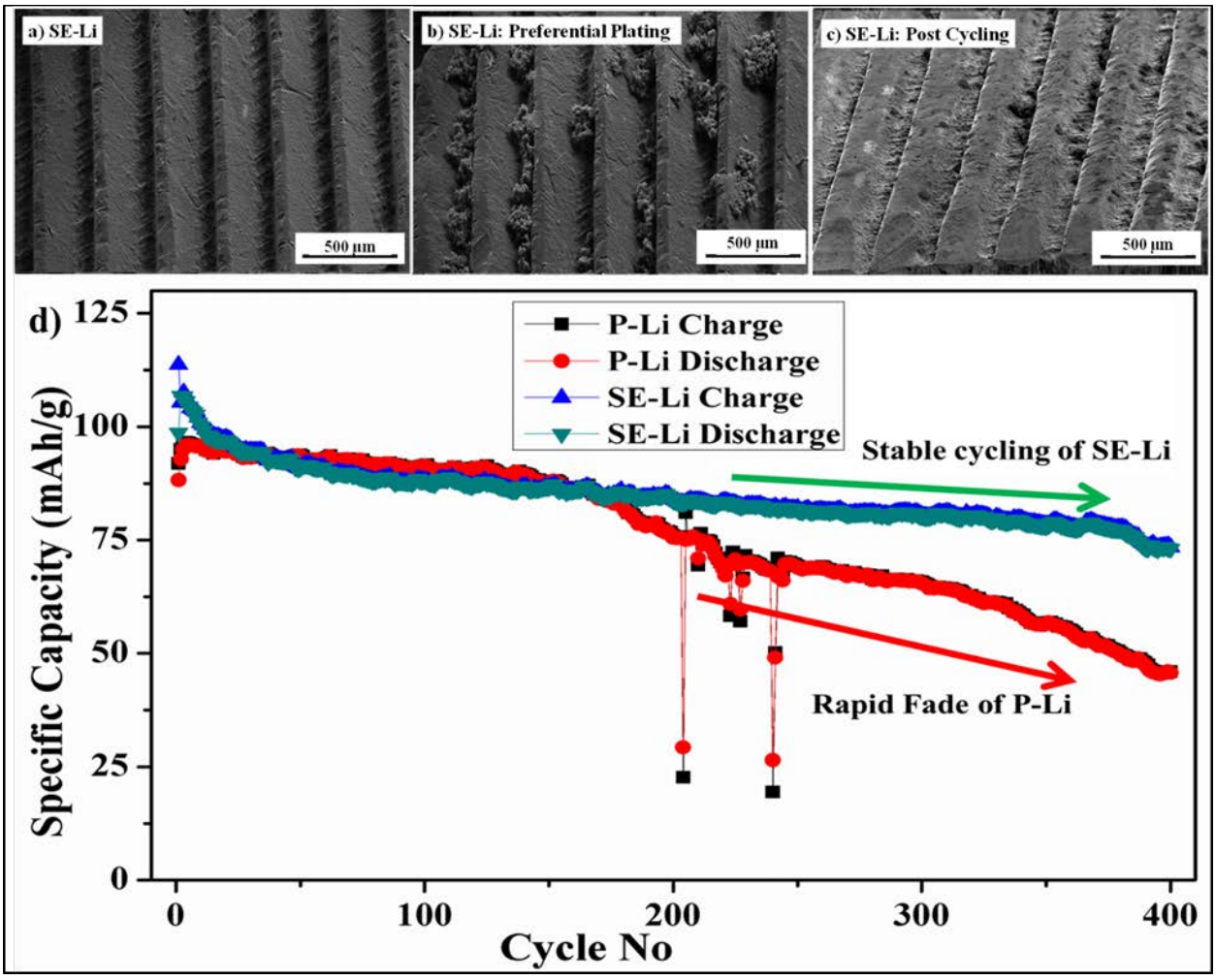

Figure 11: SEM images of a) surface engineered (SE) Lithium, b) Li plating on SE-Li and c) cycled SE-Li. d) Cycling behavior of $LiMn_2O_4$ cathode tested against P-Li and SE-Li.

Based on this observation, considerable attention has been directed towards understanding the "planar/non-planar" growth behavior of the surface engineered Li metal (SE-Li) during long term cycling. Towards this end, Sand's time analysis, post cycling SEM analysis, and full cell testing with high voltage $LiMn_2O_4$ cathode were conducted to study the planar/non-planar growth behavior of SE-Li in 1M $LiPF_6$ in EC:DEC:FEC=45:45:10 (%vol.) electrolyte. Sand's time experiment (**Figure 10b, 10c**) was conducted in a symmetric Li/Li in a three electrode Swagelok cell with SE-Li as the working electrode. The cell has been charged (Li plating) at an areal current density (I_{AD}) of 10mA/cm^2. The onsets of voltage fluctuations indicate the onset of unstable Li plating (non-planar Li growth). As shown in **Figure 10b, 10c**, pristine lithium (P-Li) and surface engineered Li (SE-Li) show fluctuations at ~60s and ~1940 s corresponding to areal charge density (Q_{AD}) of ~0.17 mAh/cm^2 and ~5.39 mAh/cm^2 respectively. The increase in the Sand's time indicates delay in the development of the high surface area mossy Li plating on SE-Li. The post plated SEM study (**Figure 11b**) of SE-Li showed preferential plating (I_{AD}=0.5mA/cm^2, t=1h) in the high energy regions due to surface engineering. P-Li under the same conditions however, shows random plating of Li. Post cycling SEM image (**Figure 11c**) of SE-Li after 10 cycles,

(I_{AD}=0.5mA/cm^2, t = 1h) shows a gradual buildup of SEI layer in the high energy regions, still retaining the engineered surface features.

Full cell cycling (**Figure 11**) of SE-Li and P-Li with $LiMn_2O_4$ cathode (~loading: 11-15 mg/cm^2) was further conducted in a coin cell cycled between 3V-4.3V at a current of 100mA/g (I_{AD}~1.5mA/cm^2) with analysis of the cycling performance. P-Li/$LiMn_2O_4$ shows rapid fade in specific capacity after 160 cycles while SE-Li/$LiMn_2O_4$ shows stable cycling till 400 cycles (**Figure 11)**. Premature capacity fade seen in P-Li electrode can be attributed to the unstable mossy plating on P-Li leading to rapid SEI layer buildup contrasted to SE-Li.

Composite Polymer Electrolyte:

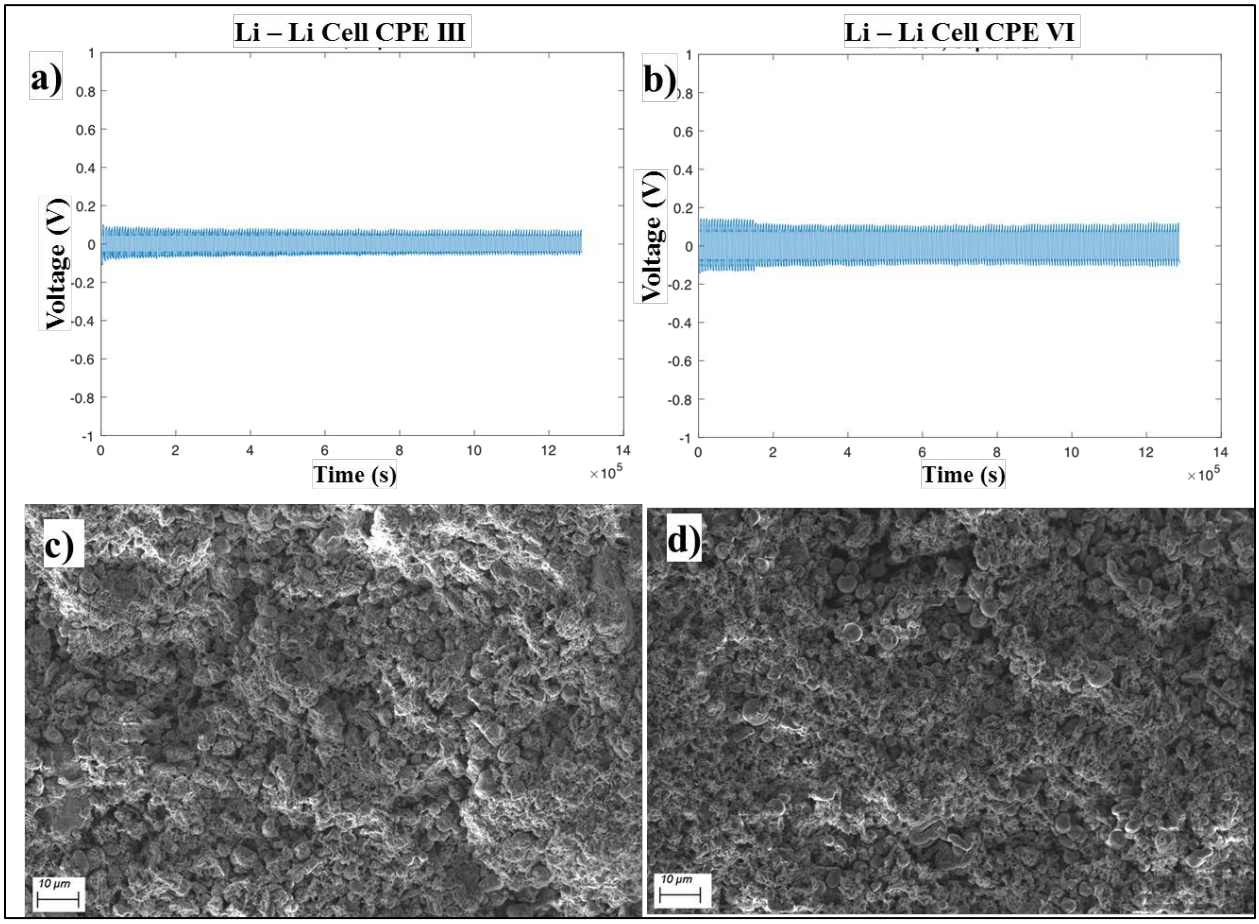

Figure 12: Voltage-time curve for symmetric Li/Li cells using composite polymer electrolytes (CPE) a) CPE-III and b) CPE-VI (~200 cycles). SEM images of lithium-metal after cycling in symmetric Li/Li cells with c) CPE-III and d) CPE-VI after ~200 cycles).

In order to stabilize the lithium-metal battery system further, studies were focused on developing a flexible moving boundary solid state electrolyte system to modify the nucleation and growth of lithium-metal on the current collector. The first approach involved development of a

composite polymer electrolyte (CPE) which would control the lithium-ion flux and thus modify the deposition conditions thereby inhibiting the dendritic growth. CPE separators were accordingly fabricated by electrospinning of polymer-blends, after which the electrospun mats were punched to yield the individual separators. The separators were then soaked in traditional liquid electrolyte (50:50 DOL:DME by volume, 1.0M LiTSFI, 0.1M $LiNO_3$) before assembling the symmetric Li/Li coin cells. No additional liquid electrolyte was added beyond that used to activate the CPEs. **Figure 12a, 12b** shows the potential-time curves generated for the two different CPEs (CPE III and CPE VI) after cycling for ~200 cycles in symmetric Li/Li cells. The SEM images collected on the lithium-metal foil after ~200 cycles indeed confirm the absence of dendrites (**Figure 12c, 12d**) and moreover indicate the formation of uniform Li metal plating due to homogenous Li^+ diffusion that is afforded by the improved Li-ion conduction processes occurring in these composite polymer electrolytes.

Zero Nucleation Potential Electrodes:

The concept of surface engineering of Li metal to control the nucleation and growth of dendritic structures was presented above. Additionally, the findings from the above study confirmed the observation that Li metal plating on Cu substrates used traditionally was unstable leading to the failure of multilayer porous Cu foams due to high nucleation potential which arises from the poor wettability of Cu with respect to Li. Hence, a significant and more in-depth study was performed in budget period 2 and 3 to identify suitable current collectors to serve as heterogeneous nucleation sites exhibiting zero or minimal nucleation barriers (i.e. zero nucleation underpotential) for Li metal plating. The heterogeneous nucleation feature described in **Figure 13a**, shows that if the contact angle between the Li metal and the current collector decreases below ~ 20º to 30º, affording improved wetting, the heterogeneous nucleation barrier, [ΔG_{cr}(het)/ΔG_{cr}(hom)], approaches almost 0, and therefore, the rate of nucleation, $J_{het,}$ is expected to increase significantly promoting uniform nucleation creating conditions for also thus effectively and favorably modifying the growth pattern. In this condition, it is expected that the nucleation underpotential for Li metal plating will be minimum leading to uniform and smooth homogeneous surface formation across the current collector if the associated contact angle is well below 30º. Furthermore, in the presence of an efficient nucleant/current collector, the columnar/needlelike growth of Li metal as well as dendrite formation can be minimized and also completely prevented by inhibiting the rapid and isotropic growth of the nucleated Li crystal.

Metal alloys as an efficient nucleant/current collector exhibiting negative heat of mixing (i.e. good wetting with Li metal) and exceptional lattice registry with Li metal have thus been identified and synthesized. **Figure 13b** shows the plating/de-plating behavior of one of the synthesized novel current collector/substrate showing "zero nucleation underpotential" tested at a current density of 0.5mA/cm^2 in the 1M $LiPF_6$ (EC:DEC) electrolyte system whereas the traditional Cu current collector exhibits large nucleation under-potential. In addition, the growth potential of Li metal (**Figure 13b**), cycled at a current density of 0.5mA/cm^2 for 1h, shows no significant change (~47 mV) with time or cycle numbers suggesting minimal Gibbs-Thomson (GT) effect on the growth potential which mainly arises due to the formation of high surface area needlelike cellular or dendritic growth of the Li metal. However, most of the efficient current

collector shows low coulombic efficiency (CE ≤90%) (**Figure 13c**) due to the irreversible side reaction of the reactive electrolyte (EC:DEC) with the current collector resulting in the formation of the solid electrolyte interphase (SEI). This adventitious side reaction in the novel materials is minimized by further alloying with non-reactive metals to inhibit SEI formation as well as forming novel "zero nucleation under-potential" binary, ternary, and multi-component alloys (MCAs). **Figure 13d** shows the preliminary results of the plating/stripping behavior of such a synthesized "zero nucleation underpotential" novel ternary alloy exhibiting high CE (>99%) tested at a charge density of 1mAh/cm^2 with a current density of 1mA/cm^2 in the EC: DEC based electrolyte. The growth front morphology of the Li metal plated at low and high current density (0.5mA/cm^2-2mA/cm^2) and charge density (0.05-4mAh/cm^2) is currently under investigation and will be reported and published in the near future.

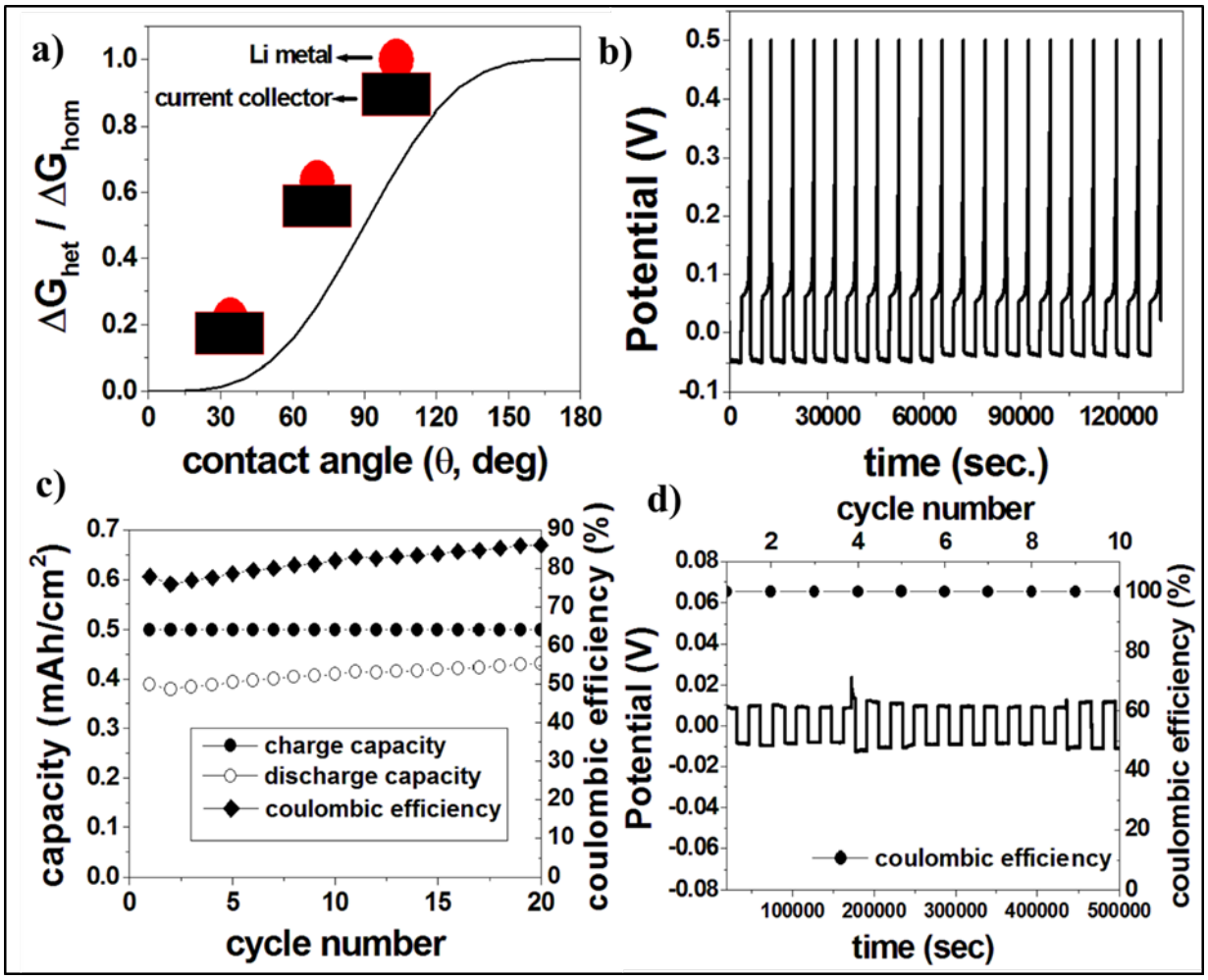

Figure 13: a) Variation of heterogeneous nucleation barrier with contact angle, b) Plating/ stripping behavior of an efficient electrode showing zero nucleation underpotential and invariant growth potential with time and cycle numbers, c) the charge/discharge capacity along with coulombic efficiency of an efficient electrode, d) Plating/stripping behavior of multicomponent alloy showing high coulombic efficiency.

A systematic theoretical and experimental study was eventually performed in the budget period 1 and 2 to understand the scientific underpinnings leading to the formation of non-planar interface

microstructure and accordingly, to determine the conditions needed for eliminating dendrite formation during Li metal plating. It is predicted that if the equilibrium potential gradient (mG_c) at the electrode/electrolyte interface arising due to concentration gradient at the interface (G_c) is higher than the true potential gradient (G_L) at the electrolyte ($mG_c > G_L$) (**Figure 14a**), the electrolyte in front of the interface will be in an underpotential state leading to a nonplanar interface.

The developed perturbation theory as well as the dendrite kinetic theory including interfacial/adhesion energy and Gibbs Thomson parameter (GTP) serve to lower the perturbation parameter in addition to the driving force for perturbation (mG_c-G_L) successfully predicting the combined effects of concentration gradient and interfacial energy on the formation of planar/non-planar interface structure. Accordingly, identification of a suitable current collector exhibiting desired adhesion energy/capillarity as well as high wettability with Li metal is thus expected to increase the energy required to perturb the interface with high curvature, and consequently, improve the cycle life of LMBs.

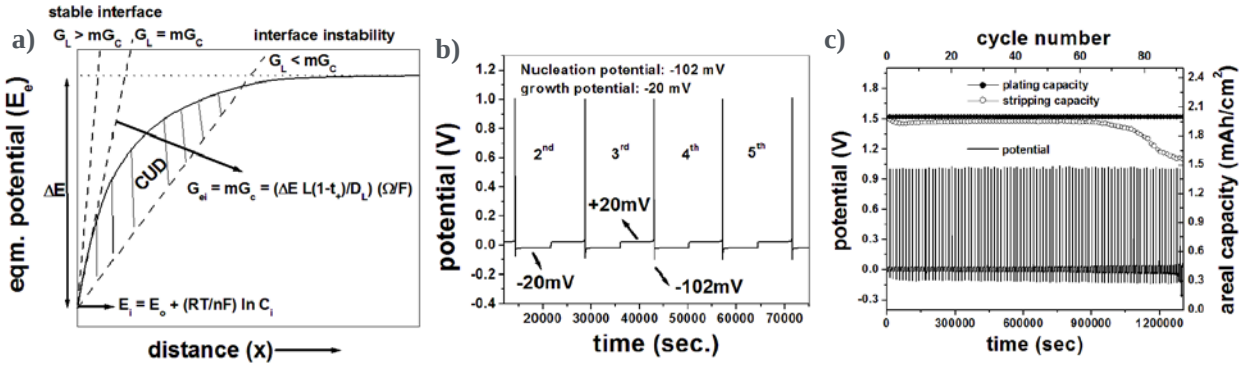

Figure 14: (a) Equilibrium plating potential of Li arising due to compositional variation at the Li-metal/electrolyte interface illustrating the condition for dendrite formation. (b) Variation of Li metal plating and stripping potential for 5th-10th cycles of positive interfacial energy current collector. The plot shows large nucleation underpotential (-100mV) with growth potential of -21mV cycled at a current density of 1mA cm^{-2} with plating areal capacity 2mAh cm^{-2} (c) Plating and stripping potential variation with time for 92 cycles, and areal capacity 2mAh/cm^2 with cycle number for positive interfacial energy current collector showing poor cycle life after 60 cycles.

It must be mentioned here that identification of suitable current collector exhibiting excellent wettability ($\theta < 30^o$, θ is wetting angle) with Li metal also improves the nucleation kinetics by minimizing the nucleation barrier and improving the nucleation rate to yield conditions for homogeneous deposition of Li metal across the current collector. Metal alloys exhibiting low interfacial energy or adhesion energy with Li metal are expected to form dendritic structures and correspondingly, delaminate from the current collector resulting in poor cycle life.

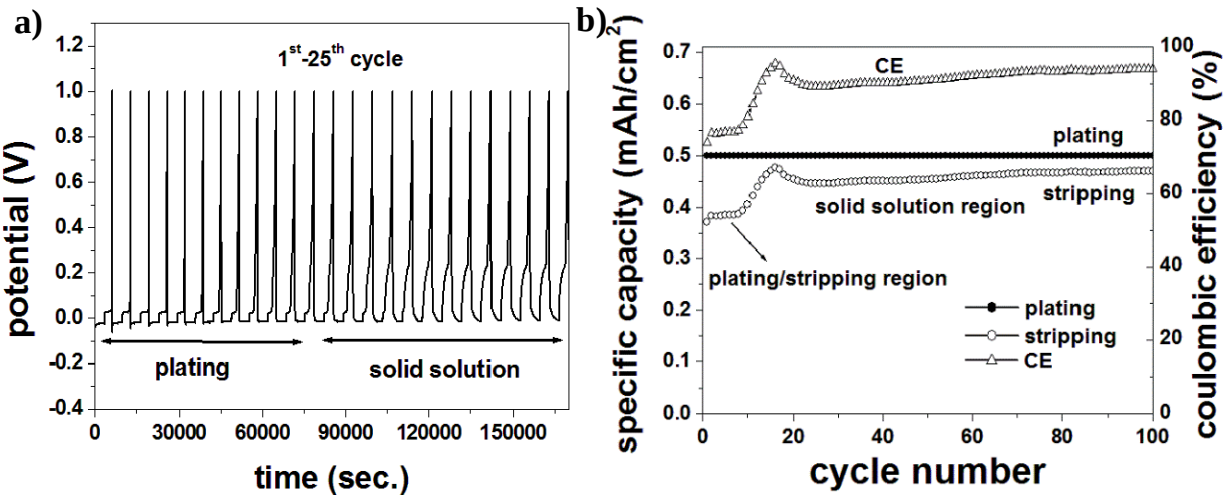

Figure 15: (a) Variation of Li metal plating and stripping potential for 25th cycles of SIA cycled at a current density of 1mA cm^{-2} with plating areal capacity 0.5mAh cm^{-2} (b) Variation areal capacity with cycle number of SIA showing excellent cycle life, however, low CE for first 10th cycles due to low Li ion diffusivity.

One of the alloys accordingly, developed by the PIs exhibiting low interfacial energy (+ 90 kJ mol^{-1}) cycled at a plating current density of 1mA cm^{-2} with a charge density 2mAh cm^{-2} shows a high nucleation underpotential (-100mV) (**Figure 14b**). The system also shows poor cycle life/coulombic efficiency after 60 cycles due to the formation of dendritic structure and subsequently causing delamination of the Li metal from the current collector (**Figure 14c**). Therefore, suitable alloy design of current collector exhibiting non-reactivity to Li metal along with high interfacial energy and excellent lattice registry as well as good wetting with Li metal is highly desirable. Several promising structurally isomorphous alloys (SIAs), multicomponent alloys (MCA) and interface engineered Cu current collectors (IES) have been developed keeping in mind the above aspects identified and generated conducive for effective Li metal plating/stripping for achieving the desired microstructural control. To determine the Li growth front morphology after significant crystal growth (~10-20μm thickness) of the nucleated Li, and study the long term cycling performance of Li metal at a charge density of 1mAh/cm^2-4mAh/cm^2, the Li metal plating/stripping was carried out at a current density of 0.5mA/cm^2-1mA/cm^2 for 1h-4h up to 100-300 cycles tested in 1.8M LiTFSI+0.2M $LiNO_3$ in DOL:DME electrolyte.

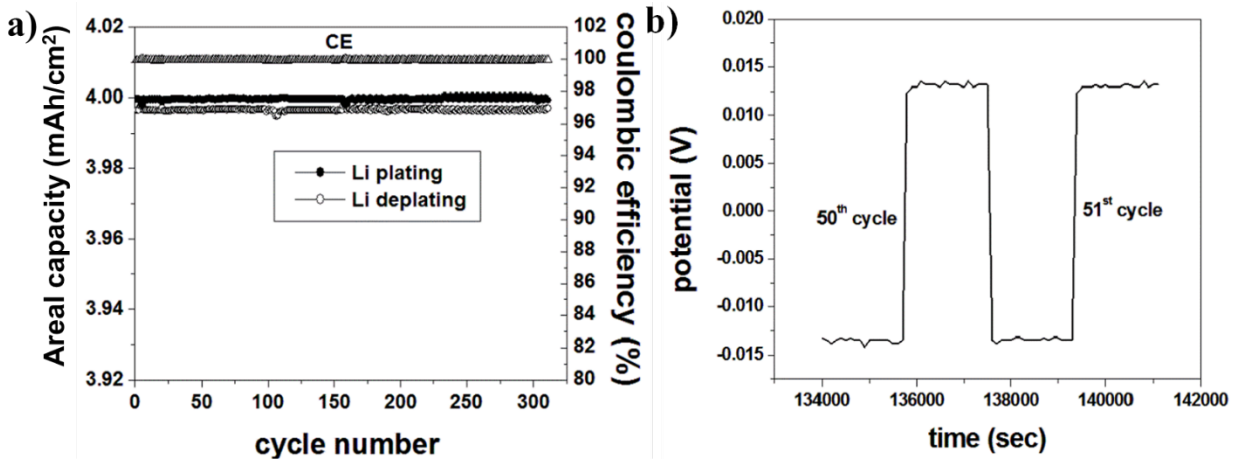

Figure 16: (a) Variation areal capacity with cycle number of MCA showing excellent cycle life with CE ~99.9% cycled at 1mA/cm^2. (b) Variation of Li metal plating and stripping potential for 50th cycles of MCA showing zero nucleation underpotential and 15mV growth potential.

The developed SIAs/MCAs/IESs with excellent Li metal lattice registry and large GTP in particular, serve as next generation current collectors displaying excellent cyclability obviating cellular or dendritic structure formation promoting long cycle life **(Figure 15, Figure 16 and Figure 17)**. SIA alloys show low CE (~80%) for first few cycles (**Figure 15**) due to low diffusivity of Li and SEI formation of highly reactive SIAs with the electrolyte. A systematic theoretical study based on DFT calculation was performed to identify suitable alloying elements to improve the Li ion diffusivity in SIA alloys. On the other hand, the developed MCA alloys show excellent cyclability upto 300 cycles with zero nucleation underpotential cycled at a current density of 1mA/cm^2 yielding an areal capacity ~4mAh/cm^2 **(Figure 16)**.

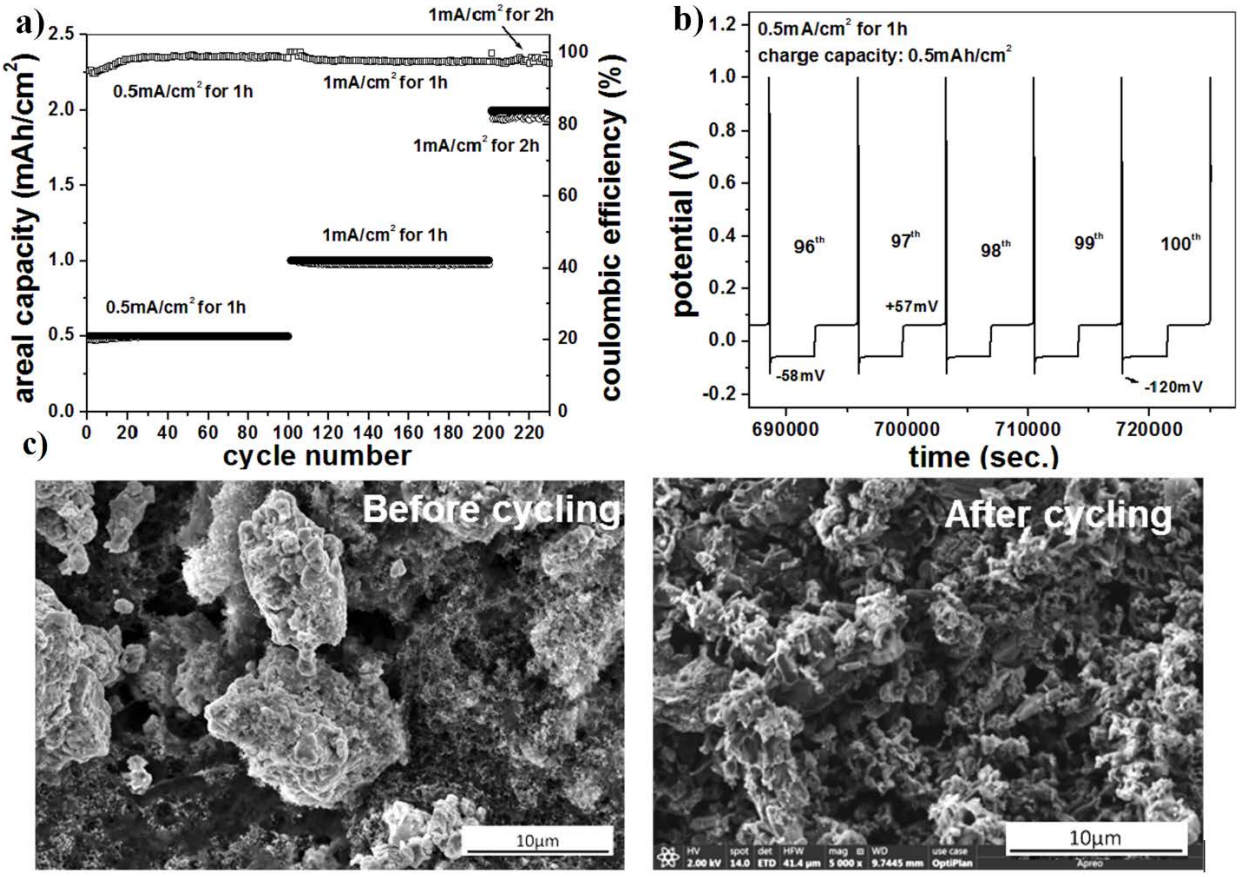

Figure 17: (a) Variation areal capacity with cycle number of IES showing excellent cycle life with CE ~99.4%. (b) Variation of Li metal plating and stripping potential for 96th-100th cycles showing 58mV growth potential. c) SEM micrograph of Li metal growth front obtained after 100 cycles.

The plating/stripping behavior of Li metal using the novel "zero nucleation underpotential" MCAs (**Figure 16**) also shows a coulombic efficiency ~100%. The SEM micrograph of the Li metal growth front obtained after 100 cycles for MCA, shown in **Figure 17c**, indicates the evolution of a planer morphology with no presence of dendritic structures. Similarly, IES on Cu current collector shows excellent cyclability (**Figure 17**). The variation of areal capacity with cycling (**Figure 17**) up to 220 cycles of studied IES coated Cu foil tested at a different current density shows excellent cyclability with CE >99.5% after 10th cycle whereas traditional Cu current collector exhibits poor cyclability after few cycles**. Figure 17b** also shows absence of intermetallics formation during Li metal plating suggesting the Li ion non-reactivity of IES to form intermetallics or solid solution. Further, the growth potential of Li metal (**Fig. 17b**), cycled at a current density of 0.5mAh/cm^2 for 1h, show no significant growth potential change (~58 mV) with time or cycling, suggesting minimal potential hysteresis of IES coated Cu foil. The above results clearly suggest that the novel materials developed exhibiting high Li ion absorption (i.e. minimizing the driving force of perturbation) and high Gibbs Thomson parameter current collector are a promising way to improve the Li metal battery performance without formation of dendrites.

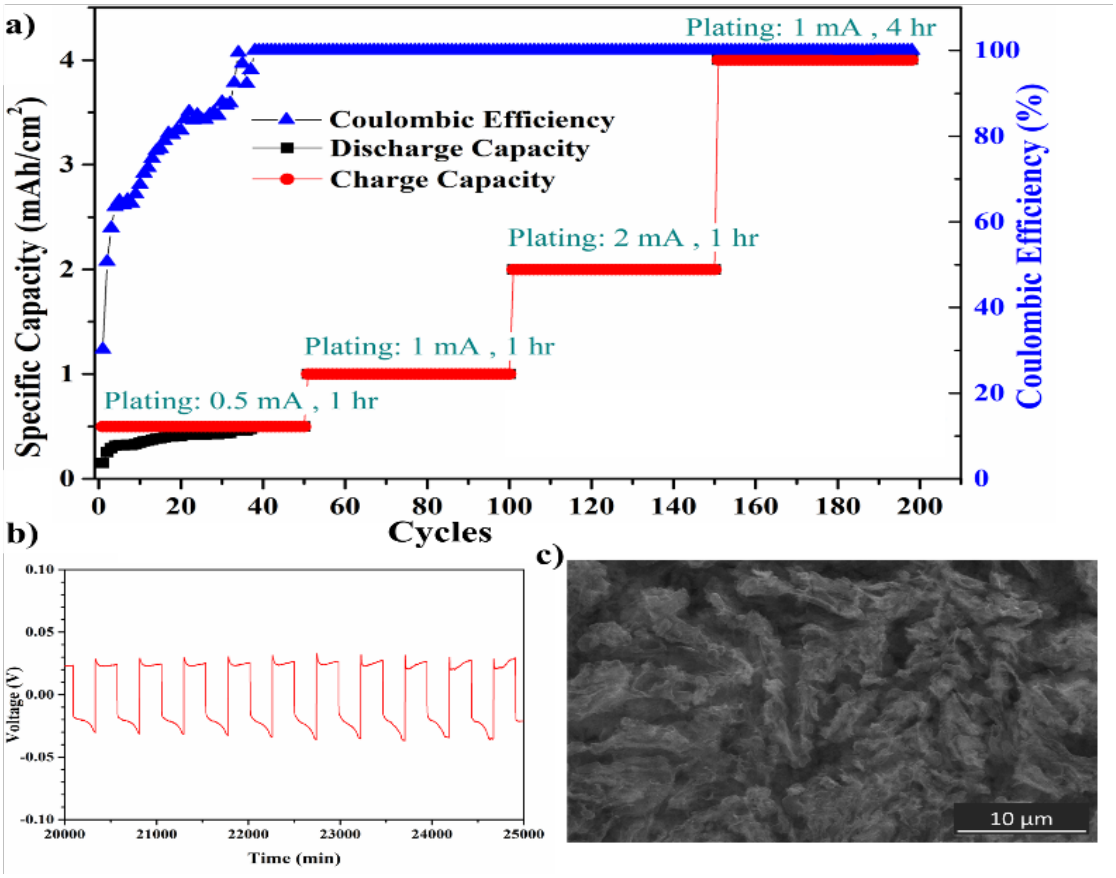

Figure 18: a) Electrochemical cycling, b) Voltage profile after 40 cycles, c) SEM after 200 cycles showing absence of dendrites, scale bar 10 microns.

In addition, different effective nucleating agents (ENA) are alloyed with effective host alloy (EHA) to form effective nucleating host alloys (ENHA) transforming the Li plating field towards uniform homogenous nucleation and growth regime. High energy mechanical milling (HEMM) was used to synthesize these new materials and the evolution of the phases was accordingly studied using X-ray diffraction. Subsequently, ENHA was studied for Li plating/stripping in a CR2025 coin cell using Li as counter/reference electrode and 1M $LiPF_6$ in EC:DEC:FEC as the electrolyte at different areal current/charge densities as shown in **Figure 18 (a)**. ENHA exhibits improvements in the electrochemical processes of reversible Li plating/stripping yielding a high coulombic efficiency of ~99.6% at the end of 200 cycles **(Figure 18a)**. The plating/stripping potential decreases ~20-40 mV as the electrode stabilizes after 40 cycles **(Figure 18b)**. Post cycled SEM images of the electrode **(Figure 18c)** indicates absence of dendrites due to the efficient nucleation and uniform growth of Li during the plating and stripping processes of ENHA alloy.

Carbon Based Nanostructures for stable lithium metal plating:

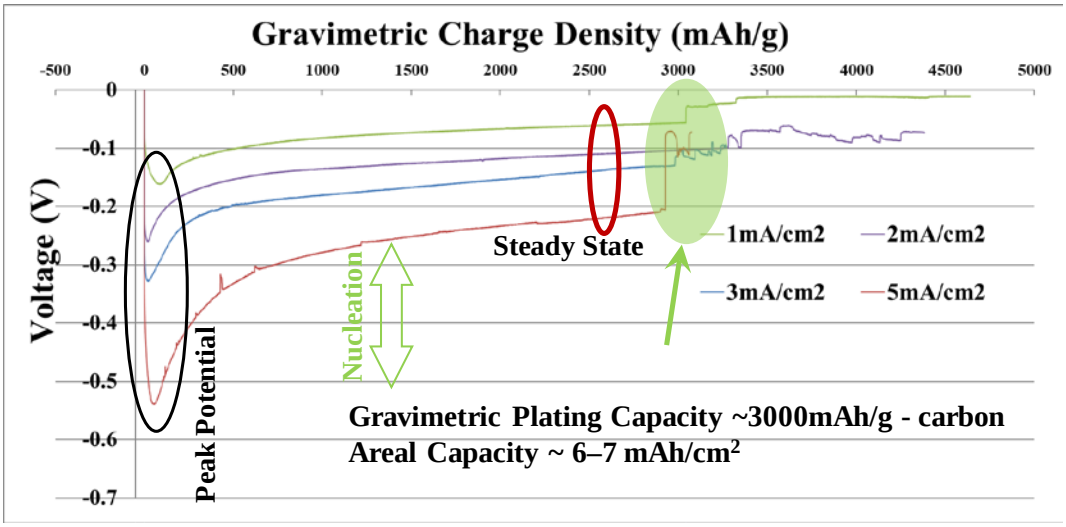

Figure 19: Nucleation and growth behavior of carbon nano -architectures at different current rates.

The major fundamental issues associated with Li plating is the high over potential of plating (both nucleation and growth) followed by inefficient electron transfer due to formation and growth of electronically non conducting SEI layer. Hence, a novel nanostructured carbon-based electrode was designed and fabricated to control the electron transfer phenomenon in the substrate and Li^+ transfer from the solvent to the growing lithium site. The surface of these nanostructured electrode provides extremely uniform deposition sites resulting in homogenous growth resulting in coalescence of growth sites and reduces the electron transfer resistance within the electrode from the surface of the Li growth site promoting uniform deposition and removal of Li metal.

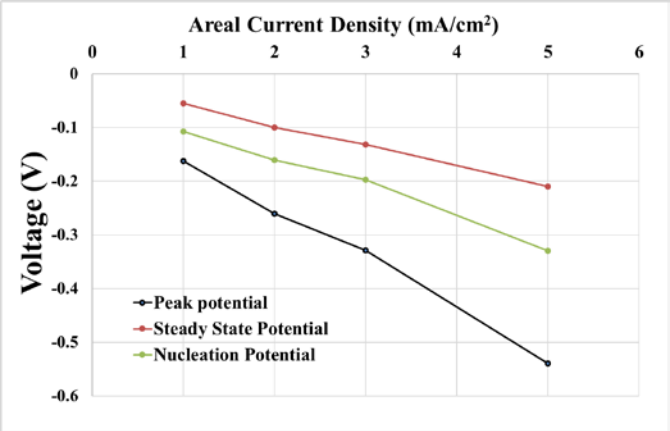

Figure 20: Variation of potentials of Li plating on carbon nanoarchitectures at different current densities.

Lithium intercalation and deintercalation reaction with these carbon-based electrodes accordingly show a capacity contribution of ~100-150mAh/g and ~40-50mAh/g at low (25mA/g) and high (4A/g) current rates, respectively, with a capacity loss of ~250-300mAh/g during the initial cycles. Subsequently, Sand's time experiment for single plating experiment was carried out in a two-electrode pressure less system to study the stability of Li plating (**Figure 19**). The electrodes show a stable plating capacity of ~3000mAh/g with an areal capacity of ~6-7mAh/cm^2 before

approaching the undesired mossy / fractal Li plating for an active material loading of ~2-3mg/cm^2. The steady state growth region shows minimal fluctuations (data point recorded @0.5mV voltage fluctuation) indicating uniform growth front. Even at high current density of 5mA/cm^2 the system shows a low nucleation overpotential ~0.33V (**Figure 20**). This carbon - based nano architecture also shows a columbic efficiency of ~95-97% during initial cycles followed by ~99.71-99.87% for over 150 cycles for a plating charge of 4mAh/cm^2 and current densities of 1mA/cm^2 and 4mA/cm^2 (**Figure 21**).

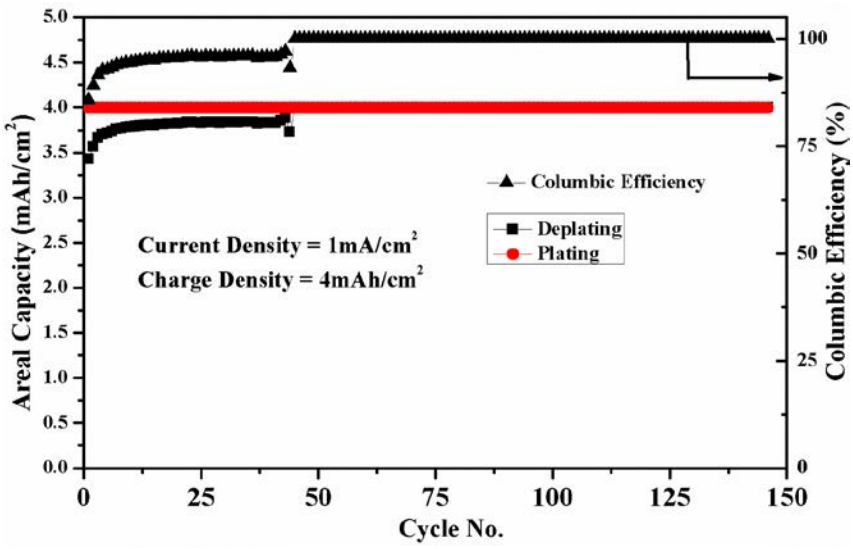

Figure 21: Columbic Efficiency of Li plating and deplating @1mA/cm^2, 4mAh/cm^2 in Li/Li$^+$ cell.

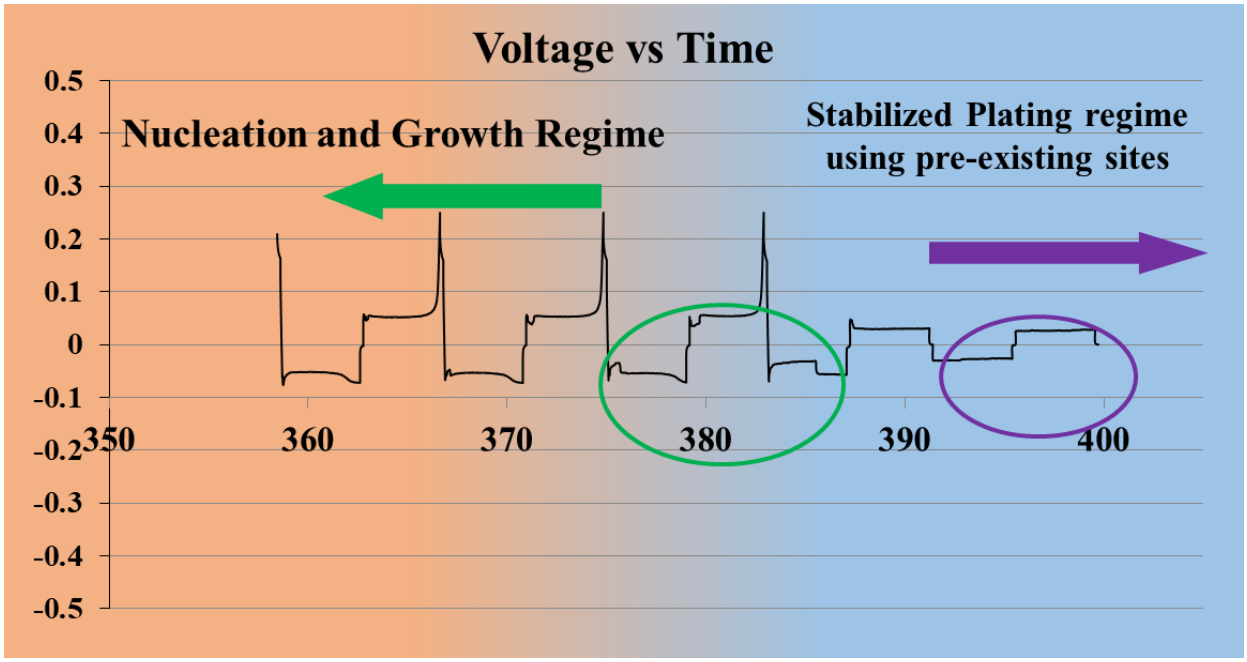

Figure 22: Voltage vs. time (hours) profile of carbon-based electrodes at the transition region in traditional coin cell testing.

Additionally, in normal coin cell testing (the Li foil area is smaller than the working copper electrode area), the Li plating hence, spreads with each cycle due to resistance to plating created by the formation of the SEI layer. Hence, a study of this transition region has been conducted to

see the votlage profile in this region for short circuiting phenomenon. A study of the voltage profile for this cell (**Figure 22**) between the 40th – 50th cycles (between 350h – 400h) indicates a distinct region with the system transitioning from nucleation and growth to plating regime without nucleation. Following this, the plating phenomenon uses pre-existing nucleation sites without creating new plating regions.

Hence, the system shows false results of stable Li plating for 30–80 cycles depending on the current/charge density. A new insulated coin cell design was introduced confining the Li plating on the copper working electrode and correspondingly, recording the actual performance of the electrodes by insulating the stainless steel in the coin cell from the electrolyte contact while preserving its electrical continuity with the copper working electrode (**Figure 23**). The CE of the Cu foil decreases to **~75 – 80%** within the first 5 cycles in the insulated coin cell compared to traditional testing where the Cu foil shows stable plating for 50 cycles. This testing method provides rapid experimental technique to study the actual performance of the materials for Li plating accelerating the study, reducing the characterization time along with providing a scientifically accurate testing method in coin cells.

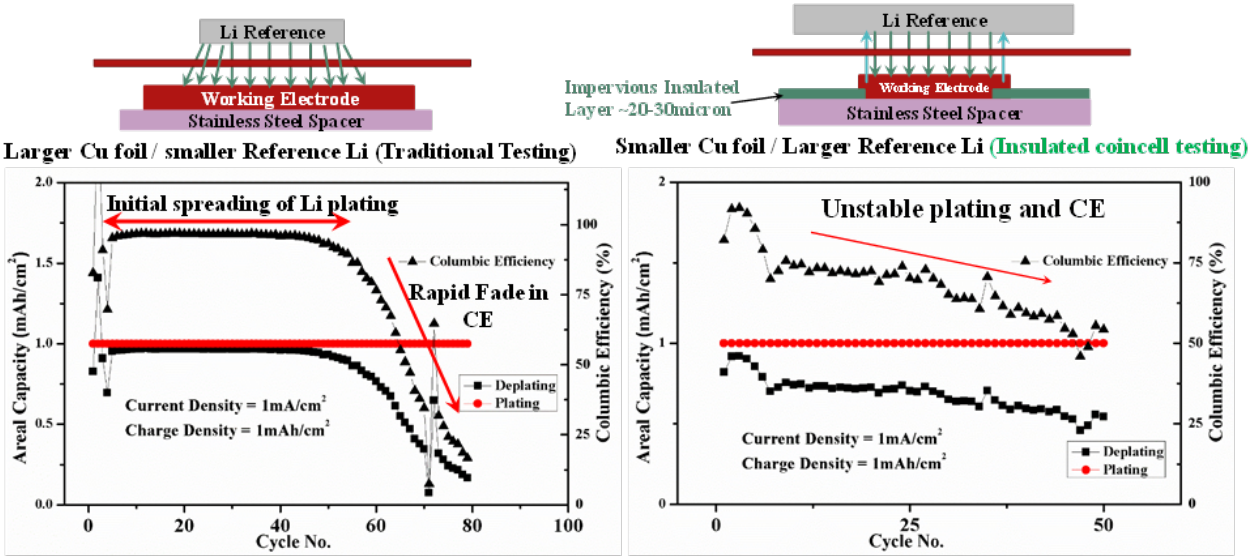

Figure 23: Schematic of the traditional and insulated coin cell testing along with the recorded performance for copper foils.

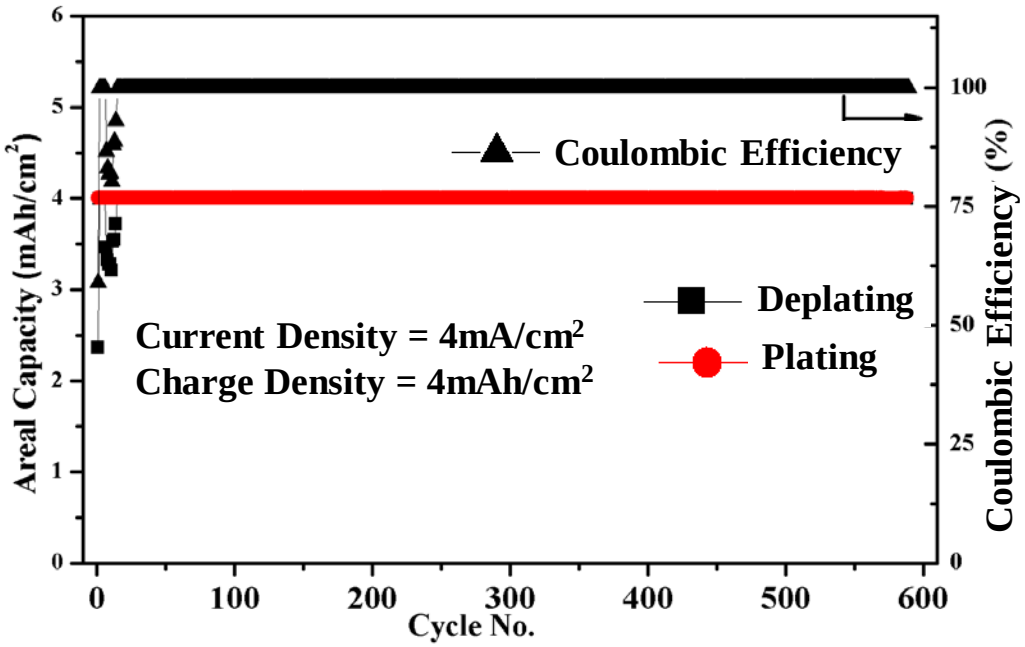

Figure 24: Columbic Efficiency of Li plating and de-plating @4mAh/cm², 4mAh/cm² in Li/Li⁺ cell (Insulated coin cell).

Hence, carbon-based architectures in traditional coin cell testing show an initial low CE of plating (~95-97%) due to spreading of the Li plating marked by distinct nucleation and growth regimes during each cycle after which the spread of Li plating saturates. Subsequently, the system shows a CE of ~99.71-99.87% representing the actual performance of the carbon nano architectures. Carbon nano – architectured electrodes thus, tested in an insulated coin cell (**Figure 24**) show a high CE of >99.85% in the first 10 cycles of Li plating and deplating @4mA/cm^2, 4mAh/cm^2 and a high CE of >99.9% for over 500 cycles upon long term cycling thus demonstrating the true potential of these carbon based innovative nanoarchitectures for serving as dendrite free anodes. CE fluctuations observed in the initial 10 cycles is due to activation of new regions in the nanostructures.

III. Project Activity Summary

Phase – 1 (budget period 1) of the current project was successful in developing porous metal foam and multilayer porous foam architectures capable of eliminating dendrite formation during cycling of lithium metal. Additionally, important modifications were made to the coin cells in order to ensure accurate testing of the studied anodes. Future work is needed to further examine the role of SEI formation on cycling stability and capacity loss. Early work has already demonstrated the ability of surface additives to control initial SEI formation and slow additional growth, resulting in extended stability. Phase – 2 of the current project continued to examine ways of addressing this problem in the porous metal foam electrodes, in addition to possible modifications to the Li-rich structurally isomorphous alloy electrodes.

Phase – 2 (budget period 2) of the current project was successful in developing organic layer embedded composite porous Cu foam architectures capable of eliminating the deleterious dendrite formation during cycling of lithium metal with stable columbic efficiency of ~96% till 130-160 cycles. The poor wettability of Cu with Li and the formation of SEI makes it an undesirable framework for plating with Li and hence, new alloy systems with enhanced wettability and lattice

registry were identified and developed to control the nucleation and growth of Li. These novel alloys developed under this approach show zero nucleation potential at a charge density of 1mAh/cm^2 with a current density of 1mA/cm^2 in EC:DEC based electrolyte with a high columbic efficiency of ~99%. Long term plating - stripping studies indicate stable growth potential of ~47mV with respect to Li/Li$^+$. Surface engineering of Li (SE-Li) metal decreases the nucleation potential and creates high energy sites for preferential plating of lithium thus improving the performance in LIBs. The improvement in the performance of SE-Li was observed in terms of Sands time, post cycling SEM analysis after repeated Li plating/deplating followed by full cell studies using $LiMn_2O_4$ as the cathode with plating/deplating charge densities of ~1.4-1.5mAh/cm^2. Composite polymer electrolytes were developed as a part of electrolyte modification using electrospinning of various blend polymers with novel ceramic fillers to induce controlled Li flux during plating and deplating. The symmetric Li cells cycled using these CPEs showed no change in plating / deplating overpotentials till 200 cycles in a Li/Li symmetric cell with complete absence of dendritic Li plating as indicated in the post cycling SEM analysis.

In budget period 3, a rigorous theoretical study based on mass transfer and charge transfer of Li ions under the combined influence of potential gradient (G_L), named as migrational Li ion flux, and concentration gradient (G_c), named as diffusional flux, has been conducted. It is predicted that if the equilibrium potential gradient generated at the electrode/electrolyte interface ($G_L = mG_c$) arising due to concentration gradient at the interface is higher than the true potential gradient in the electrolyte ($mG_c > G_L$), the electrolyte in front of the interface will be in an underpotential region and as a result, a non-planar interface will be formed. In addition to the driving force to perturbation (mG_c-G_L) parameter, the developed perturbation theory as well as dendrite kinetic theory successfully predicts the effect of interfacial energy (γ) or Gibbs Thomson parameter (Γ) as resistance to the perturbation parameter on the formation of planar interface structure. The detailed theoretical analysis herein brings to the forefront the intricate connections between the concentration and the potential gradients with the current density such that one can predict, modify, and control the microstructure of the electrochemically deposited Li metal by designing appropriate current collectors, electrolyte and cycling conditions to prevent the deleterious influence of formation of dendrites thus even enabling an anode-free LMB system. Identification of such suitable current collectors, exhibiting desired interfacial energy/capillarity with Li metal (high Gibbs Thomson parameter (Γ)) are in line with the theoretical analyses, and as a result, offer a novel approach to dendrite-free anode less LMB system with improved cycle life.
The current project was therefore successful in developing several systems (SIA, MCA, IES, ENHA) exhibiting zero nucleation underpotential and no intermetallic formation with the Li metal. The developed alloys clearly suggest a pathway that novel materials exhibiting high Li ion absorption (i.e. minimizing the driving force of perturbation) and high Gibbs Thomson parameter current collector can be generated which are a promising way to improve the Li metal battery performance without formation of dendrites over long cycles (~300 cycles). Additionally, novel nanostructured carbon electrode structures were developed along with an accurate framework for electrode fabrication combined with the electrochemical characterization of the Li plating and deplating processes. These carbon - based nanostructures showed a high columbic efficiency of ~99.71-99.87% for over 500 cycles when tested in insulated coin cell at current densities of ~1 – 6 mA/cm^2 and areal charge densities of 4 – 6 mAh/cm^2.

IV. Products Developed / Technology Transfer Activities

Not Applicable

V. Computer Modeling

Not Applicable